

# Lyman continuum leaking from the compact star-forming dwarf galaxy J0925+1403

Y. I. Izotov<sup>1</sup>, I. Orlitová<sup>2</sup>, D. Schaerer<sup>3,4</sup>, T. X. Thuan<sup>5</sup>, A. Verhamme<sup>3</sup>, N. G. Guseva<sup>1</sup> & G. Worseck<sup>6</sup>

<sup>1</sup> Main Astronomical Observatory, National Academy of Sciences of Ukraine, 27 Zabolotnoho str., Kyiv 03680, Ukraine

<sup>2</sup> Astronomical Institute, Czech Academy of Sciences, Boční II 1401, 141 00, Prague, Czech Republic

<sup>3</sup> Observatoire de Genève, Université de Genève, 51 Ch. des Maillettes, 1290, Versoix, Switzerland

<sup>4</sup> CNRS, IRAP, 14 Avenue E. Belin, 31400 Toulouse, France

<sup>5</sup> Astronomy Department, University of Virginia, PO Box 400325, Charlottesville, VA 22904, USA

<sup>6</sup> Max-Planck-Institut für Astronomie, Königstuhl 17, 69117 Heidelberg, Germany

**One of the key questions in observational cosmology is the identification of the sources responsible for ionisation of the Universe after the cosmic Dark Ages, when the baryonic matter was neutral. The currently identified distant galaxies are insufficient to fully reionise the Universe by redshift  $z \sim 6^{1-3}$ , but low-mass star-forming galaxies are thought to be responsible for the bulk of the ionising radiation<sup>4-6</sup>. Since direct observations at high redshift are difficult for a variety of reasons, one solution is to identify local proxies of this galaxy population. However, starburst galaxies at low redshifts are generally opaque to their ionising radiation<sup>7-9</sup>. This radiation with small escape fractions of  $\sim 1-3\%$  is directly detected only in three low-redshift galaxies<sup>10,11</sup>. Here we present far-ultraviolet observations of a nearby low-mass star-forming galaxy, J0925+1403, selected for its compactness and high excitation. The galaxy is leaking ionising radiation, with an escape fraction of  $\sim 8\%$ . The total number of photons emitted during the starburst phase is sufficient to ionize intergalactic medium material, which is about 40 times more massive than the stellar mass of the galaxy.**

So-called “Green Peas” (GP), low-mass compact galaxies with very active star formation<sup>12-15</sup>, may be promising candidates for escaping ionising radiation. The GP galaxy J0925+1403 was selected from the Sloan Digital Sky Survey (SDSS) according to the following properties (Methods section): 1) a compact structure; 2) the presence of emission lines with high equivalent widths in its SDSS spectrum, suggesting active ongoing star formation and numerous hot O stars producing ionising Lyman continuum (LyC) radiation; 3) sufficiently bright in the far-ultraviolet (FUV) with a magnitude of 20.7 mag and redshifted enough ( $z = 0.301$ ) to allow direct LyC observations with the Cosmic Origins Spectrograph (COS) onboard the Hubble Space Telescope (HST); and 4) a high  $O_{32} = [\text{OIII}]\lambda 5007/[\text{OII}]\lambda 3727$  flux ratio of 5 (see Fig. 1), which may indicate the presence of density-bounded HII regions<sup>16</sup>, i.e. escaping LyC radiation.

We first derive some general properties of the galaxy, using the emission-line fluxes measured from the SDSS optical spectrum. After correction for the Milky Way extinction of  $A_{V,MW} = 0.084$  mag, we obtain an internal extinction  $A_{V,int} = 0.36$  mag, and a low oxygen abundance  $12 + \log O/H = 7.91 \pm 0.03$ , or less than 0.2 solar. The details of these determinations are given in the Methods

section. Everywhere in the paper the errors are  $1\sigma$  errors.

The same SDSS spectrum is used to fit a spectral energy distribution (SED) to derive the galaxy's global parameters, including the stellar mass and the age of the present burst of star formation (see Methods section). We obtain a starburst age of  $2.6 \pm 0.2$  Myr, a young stellar mass of  $(2.4 \pm 0.3) \times 10^8 M_\odot$ , and a total galaxy stellar mass of  $(8.2 \pm 0.7) \times 10^8 M_\odot$ . The star-formation rate is  $52.2 M_\odot \text{ yr}^{-1}$ , as determined from the extinction-corrected  $H\beta$  line flux. With its low mass, low metallicity, low extinction, compact morphology, and high star-formation rate, J0925+1403 shares many of the properties of high-redshift Lyman Alpha Emitters.

GPs with  $O_{32} \geq 5$  have been observed before by HST<sup>18,19</sup>, but their low redshifts  $z < 0.3$  were not optimal for LyC observations. The HST/COS observations of J0925+1403 were obtained on 28 March, 2015 (program GO13744, PI: T. X. Thuan). The near-ultraviolet (NUV) acquisition image shows the galaxy to have a very compact structure, with a half-light angular diameter of  $\sim 0.2''$ , much smaller than the spectroscopic aperture of  $2.5''$  (Fig. 2). This angular diameter corresponds to a linear diameter of  $\sim 1$  kpc at the angular diameter distance of 930 Mpc, derived from the redshift  $z = 0.301$ , adopting the Planck mission cosmological parameters  $H_0 = 67.1 \text{ km s}^{-1} \text{ Mpc}^{-1}$ ,  $\Omega_\lambda = 0.682$  and  $\Omega_m = 0.318$ <sup>20</sup>.

Spectra of J0925+1403 were obtained with two gratings. The low-resolution G140L grating ( $<900 - 2385 \text{ \AA}$ ) was used to obtain the spectrum, which includes the redshifted LyC emission, with an exposure time of 5649 s. The medium-resolution G160M grating ( $1410 - 1796 \text{ \AA}$ ) was used to obtain the spectrum, which includes the redshifted  $\text{Ly}\alpha \lambda 1216 \text{ \AA}$  line, with the exposure time of 2978 s. The observations with the G160M and G140L gratings were reduced with the standard pipeline and custom software, respectively. The custom software gives more accurate results, as it is specifically designed for faint HST/COS targets (see Methods section).

A strong  $\text{Ly}\alpha \lambda 1216 \text{ \AA}$  emission-line is detected in the medium-resolution spectrum. Its profile (Fig. 3) shows two peaks on both sides of the line center (dashed vertical line). According to radiative transfer models, the separation between the  $\text{Ly}\alpha$  line peaks increases with increasing optical depth and thus with increasing neutral hydrogen column density  $N(\text{HI})$ <sup>21</sup>. In the case of J0925+1403, the separation of  $\sim 300 \text{ km s}^{-1}$  corresponds to a low column density ( $\log N(\text{HI}) \leq 10^{19} \text{ cm}^{-2}$ ), allowing the escape of a considerable fraction of the  $\text{Ly}\alpha$  emission. Correcting for the Milky Way and galaxy internal reddening we obtain a  $\text{Ly}\alpha$  flux density of  $8.2 \times 10^{-14} \text{ erg s}^{-1} \text{ cm}^{-2}$ . Comparing the extinction-corrected  $\text{Ly}\alpha/H\beta$  flux ratio of  $16.7 \pm 1.0$  and case B flux ratio of  $23.3$ <sup>22</sup>, we find that the  $\text{Ly}\alpha$  escape fraction is  $\sim 70\%$ , among the highest known so far for GP galaxies<sup>19</sup>, and consistent with a low HI column density.

The short-wavelength part of the J0925+1403 spectrum, obtained with the low-resolution grating G140L, is shown in Fig. 4a by the grey solid line. The modelled UV SED of the young cluster with the age and extinction parameters obtained before from SED fitting in the optical range (see Method section) is shown by the black solid line. We adopt the reddening curve<sup>23</sup>, corresponding to  $R_{V,\text{MW}} = A_V/E_{B-V} = 3.1$  for the Milky Way and to  $R_{V,\text{int}} = 2.4$  for J0925+1403, except for  $\lambda \leq 1250 \text{ \AA}$ , where the reddening curve<sup>24</sup> is used. The corresponding intrinsic spectral energy distribution is shown in Fig. 4a by the black dash-dotted line. The flux density of the intrinsic Lyman continuum is determined primarily by the extinction-corrected flux density of the  $H\beta$  emission line and the starburst age. The starburst age is derived from the condition that the

observed equivalent width of the  $H\beta$  emission line is equal to the modelled value, which depends on the extinction-corrected flux of the continuum near  $H\beta$  and the intrinsic LyC flux. The intrinsic LyC is fairly insensitive to the adopted stellar evolution models, stellar atmosphere models and initial mass function (see Method section). It is seen that the reddened SED reproduces very well the observed spectrum for rest-frame wavelengths  $> 912\text{\AA}$ .

Fig. 4b shows a blow-up of the LyC spectral region. The important feature to note is that the Lyman continuum flux density for  $\lambda < 912\text{\AA}$  is not zero, but positive with a value equal to  $(2.35\pm 0.20)\times 10^{-17} \text{ erg s}^{-1} \text{ cm}^{-2} \text{ \AA}^{-1}$ , when averaged over the  $861 - 907 \text{ \AA}$  rest-frame spectral range. It is detected at the  $11.6\sigma$  level and is indicated by a dotted horizontal line and a filled circle in Fig. 4b. This observed LyC should be corrected for the Milky Way extinction before the determination of the LyC escape fraction. The extinction-corrected average LyC flux density of  $(3.43\pm 0.29)\times 10^{-17} \text{ erg s}^{-1} \text{ cm}^{-2} \text{ \AA}^{-1}$  is shown by the thick solid horizontal line (Fig. 4b). Comparing this value to the intrinsic continuum flux density of  $4.4\times 10^{-16} \text{ erg s}^{-1} \text{ cm}^{-2} \text{ \AA}^{-1}$  beyond the Lyman limit for  $\lambda < 912 \text{ \AA}$ , we obtain an absolute LyC escape fraction  $f_{\text{esc}} = 7.8\% \pm 1.1\%$  in J0925+1403, where the error is determined by the observed LyC flux density error and uncertainties in the modelled intrinsic LyC flux density. This value is several times higher than  $f_{\text{esc}}$  of the other three low-redshift galaxies with known LyC leakage. J0925+1403 also has the highest [OIII]/[OII] flux ratio, the lowest metallicity and the lowest stellar mass. Thus we conclude that compact low-mass star-forming galaxies with high [OIII]/[OII] ratios may lose a considerable fraction of their LyC emission to the IGM.

The above determination of  $f_{\text{esc}}$  holds for UV-emitting star-forming regions without dust-obscured star formation, which is invisible in the UV and/or optical ranges. The sky region containing the galaxy J0925+1403 has been observed in the mid-infrared range by the Wide-field Infrared Survey Explorer (WISE). However, data for this galaxy are not present in the AllWISE Source Catalog<sup>25</sup>. There are also no data in the radio range. Optical, near- and mid-infrared observations of other low-metallicity star-forming galaxies with similar properties suggest that they are relatively transparent<sup>26</sup>. Negligible dust-obscured star formation is also implied by the observed thermal free-free cm radio emission in dwarf galaxies with optical and infrared observations as it is consistent with the value derived from the flux density of the  $H\beta$  emission line<sup>27</sup>. Presumably, the same conclusion holds for J0925+1403.

The number of ionising photons escaping the galaxy is  $Q_{\text{H}} = 3.86\times 10^{53} \text{ s}^{-1}$  if  $f_{\text{esc}} = 7.8\%$  (Methods section), corresponding to a total number of ionising photons of  $3.6\times 10^{67}$  emitted during a starburst with a 3 Myr duration. This total number of photons is sufficient to ionise the low-density IGM gas with a mass of  $\sim 4\times 10^{10} M_{\odot}$ , or about 40 times higher than the stellar mass of the galaxy, assuming one photon suffices to ionise one hydrogen atom. Here we adopt the luminosity distance of 1620 Mpc. Finally, we note that our galaxy leaks a large number of ionising photons per UV luminosity,  $Q_{\text{H}}/L_{1500} \approx 10^{25} \text{ photon s}^{-1}/(\text{ergs s}^{-1}\text{Hz}^{-1})$ , approximately three times more, than (optimistic) assumptions<sup>1</sup> used at high redshift for  $f_{\text{esc}} = 0.2$ , which is primarily due to the young age of the UV-dominant stellar population in J0925+1403.

**Online Content** Methods, along with any additional Extended Data display items and Source Data, are available in the online version of the paper; references unique to these sections appear only in the online paper.

## References

1. Robertson, B. E. *et al.* New Constraints on Cosmic Reionisation from the 2012 Hubble Ultra Deep Field Campaign. *Astrophys. J.* **768**, 71 (2013).
2. Steidel, C. C., Pettini, M. & Adelberger, K. L. Lyman-Continuum Emission from Galaxies at  $z \geq 3.4$ . *Astrophys. J.* **546**, 665–671 (2001).
3. Iwata, I. *et al.* Detections of Lyman Continuum from Star-Forming Galaxies at  $z \sim 3$  through Subaru/Suprime-Cam Narrow-Band Imaging. *Astrophys. J.* **692**, 1287–1293 (2009).
4. Mitra, S., Ferrara, A. & Choudhury, T. R. The escape fraction of ionising photons from high-redshift galaxies from data-constrained reionisation models. *Mon. Not. R. Astron. Soc.* **428**, L1–L5 (2013).
5. Yajima, H., Choi, J.-H. & Nagamine, K. Escape fraction of ionising photons from high-redshift galaxies in cosmological SPH simulations. *Mon. Not. R. Astron. Soc.* **412**, 411–422 (2011).
6. Wise, J. H. & Cen, R. Ionising Photon Escape Fractions From High-Redshift Dwarf Galaxies. *Astrophys. J.* **693**, 984–999 (2009).
7. Leitherer, C., Ferguson, H. C., Heckman, T. M. & Lowenthal, J. D. The Lyman Continuum in Starburst Galaxies Observed with the Hopkins Ultraviolet Telescope. *Astrophys. J.* **454**, L19–L22 (1995).
8. Deharveng, J.-M. *et al.* Constraints on the Lyman continuum radiation from galaxies: First results with FUSE on Mrk 54. *Astron. & Astrophys.* **375**, 805–813 (2001).
9. Grimes, J. P. *et al.* Observations of Starburst Galaxies With Far-Ultraviolet Spectrographic Explorer: Galactic Feedback in the Local Universe. *Astrophys. J. Suppl.* **181**, 272–320 (2009).
10. Leitet, E., Bergvall, N., Hayes, M., Linné, S. & Zackrisson, E. Escape of Lyman continuum radiation from local galaxies. Detection of leakage from the young starburst Tol 1247-232. *Astron. & Astrophys.* **553**, A106 (2013).
11. Borthakur, S., Heckman, T. M., Leitherer, C. & Overzier, R. A. A local clue to the reionisation of the universe. *Science* **346**, 216–219 (2014).
12. Cardamone, C. *et al.* Galaxy Zoo Green Peas: discovery of a class of compact extremely star-forming galaxies. *Mon. Not. R. Astron. Soc.* **399**, 1191-1205 (2009).
13. Izotov, Y. I., Guseva, N. G. & Thuan, T. X. Green Pea Galaxies and Cohorts: Luminous Compact Emission-line Galaxies in the Sloan Digital Sky Survey. *Astrophys. J.* **728**, 161 (2011).
14. Jaskot, A. E. & Oey, M. S. The Origin and Optical Depth of Ionising Radiation in the "Green Pea" Galaxies. *Astrophys. J.* **766**, 91 (2013).

15. Stasińska, G., Izotov, Y., Morisset, C. & Guseva, N. Excitation properties of galaxies with the highest [OIII]/[OII] ratios. No evidence for massive escape of ionising photons. *Astron. & Astrophys.* **576**, A83 (2015).
16. Nakajima, K. & Ouchi, M. Ionisation state of inter-stellar medium in galaxies: evolution, SFR- $M_*$  -  $Z$  dependence, and ionising photon escape. *Mon. Not. R. Astron. Soc.* **442**, 900–916 (2014).
17. Izotov, Y. I., Guseva, N. G., Fricke, K. J. & Henkel, C. Multi-wavelength study of 14 000 star-forming galaxies from the Sloan Digital Sky Survey. *Astron. & Astrophys.* **561**, A33 (2014).
18. Jaskot, A. E. & Oey, M. S. Linking Ly $\alpha$  and Low-ionisation Transitions at Low Optical Depth. *Astrophys. J.* **791**, L19 (2014).
19. Henry, A., Scarlata, C., Martin, C. S. & Erb, D. Ly $\alpha$  emission from Green Peas: the role of circumgalactic gas density, covering, and kinematics. *Astrophys. J.* **809**, 19 (2015).
20. Planck Collaboration. Planck 2013 results. XVI. Cosmological parameters. *Astron. & Astrophys.* **571**, A16 (2014).
21. Verhamme, A., Orlitová, I., Schaerer, D. & Hayes, M. Using Lyman- $\alpha$  to detect galaxies that leak Lyman continuum. *Astron. & Astrophys.* **578**, A7 (2015).
22. Hummer, D. G. & Storey, P. J. Recombination-line intensities for hydrogenic ions. I - Case B calculations for HI and HeII. *Mon. Not. R. Astron. Soc.* **224**, 801–820 (1987).
23. Cardelli, J. A., Clayton, G. C. & Mathis, J. S. The relationship between infrared, optical, and ultraviolet extinction. *Astrophys. J.* **345**, 245–256 (1989).
24. Mathis, J. S. Interstellar dust and extinction. *Ann. Rev. Astron. Astrophys.* **28**, 10–90 (1990).
25. Wide-field Infrared Survey Explorer (WISE) and NEOWISE. <http://irsa.ipac.caltech.edu/Missions/wise.html> (2013).
26. Izotov, Y. I. & Thuan, T. X. Near-infrared Spectroscopy of Five Blue Compact Dwarf Galaxies: II Zw 40, Mrk 71, Mrk 930, Mrk 996, and SBS 0335-052E. *Astrophys. J.* **734**, 82 (2011).
27. Izotov, Y. I., Guseva, N. G., Fricke, K. J., Krügel, E. & Henkel, C. Dust emission in star-forming dwarf galaxies: General properties and the nature of the submm excess. *Astron. & Astrophys.* **570**, A97 (2014).

**Acknowledgements** Based on observations made with the NASA/ESA Hubble Space Telescope, obtained from the data archive at the Space Telescope Science Institute. STScI is operated by the Association of Universities for Research in Astronomy, Inc. under NASA contract NAS 5-26555. Support for this work was provided by NASA through grant number HST-GO-13744.001-A from the Space Telescope Science Institute, which is operated by AURA, Inc., under NASA contract NAS 5-26555. I.O. acknowledges a grant GACR 14-20666P. The SDSS is managed by the Astrophysical Research Consortium for

the Participating Institutions. GALEX is a NASA mission managed by the Jet Propulsion Laboratory. This research has made use of the NASA/IPAC Extragalactic Database (NED) which is operated by the Jet Propulsion Laboratory, California Institute of Technology, under contract with the National Aeronautics and Space Administration.

**Author Contribution** All authors participated at the design of the HST observational program. Y.I.I. and N.G.G. selected the galaxy sample. T.X.T. and Y.I.I. lead the observations. G.W. reduced the HST data. I.O. did part of the HST data analysis. Y.I.I. and D.S. did the SED modelling and interpretation. A.V. and Y.I.I. did the  $Ly\alpha$  interpretation. The bulk of the text was written by Y.I.I. All authors commented on the manuscript at all stages.

**Competing Interests** Reprints and permissions information is available at [www.nature.com/reprints](http://www.nature.com/reprints). The authors declare no competing financial interests.

**Correspondence** Correspondence should be addressed to Y.I.I. (email: [izotov@mao.kiev.ua](mailto:izotov@mao.kiev.ua)).

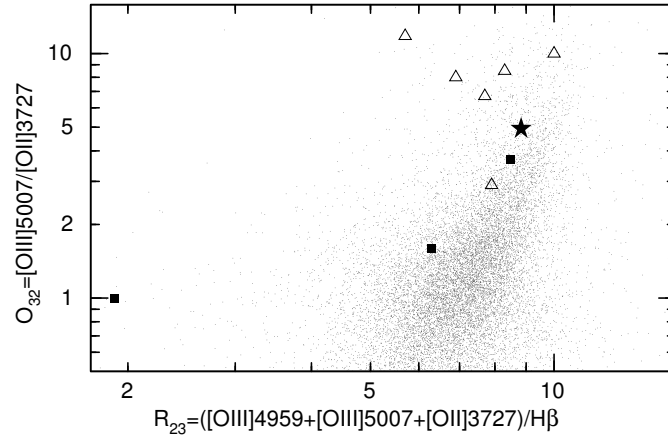


**Figure 1 | The  $O_{32} - R_{23}$  diagram for star-forming galaxies.** The quantity  $R_{23}$  is the total flux of the strongest oxygen lines in the optical spectrum relative to  $H\beta$ . This quantity is used for easier comparison with high-redshift LAEs potentially leaking ionizing radiation<sup>16</sup>, shown by open triangles. At low metallicities  $12 + \log O/H < 8.3$   $R_{23}$  increases with the metallicity. The location of J0925+1403 and known low-redshift LyC leaking galaxies<sup>10,11</sup> are shown by filled star and filled squares, respectively. SDSS star-forming galaxies<sup>17</sup> are represented by dots.

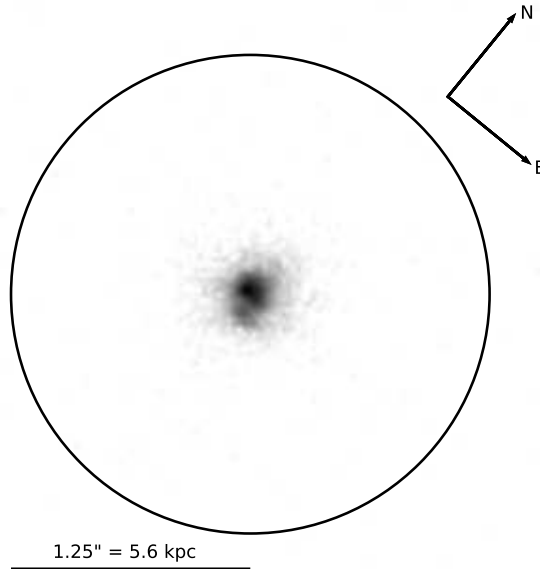


**Figure 2 | The Hubble Space Telescope near-ultraviolet image of J0925+1403.** The galaxy with a linear diameter  $\sim 2$  kpc consists of two compact star-forming regions superimposed on an extended low-surface-brightness component. The spectroscopic aperture with a diameter of  $2.5''$  is shown by a circle.

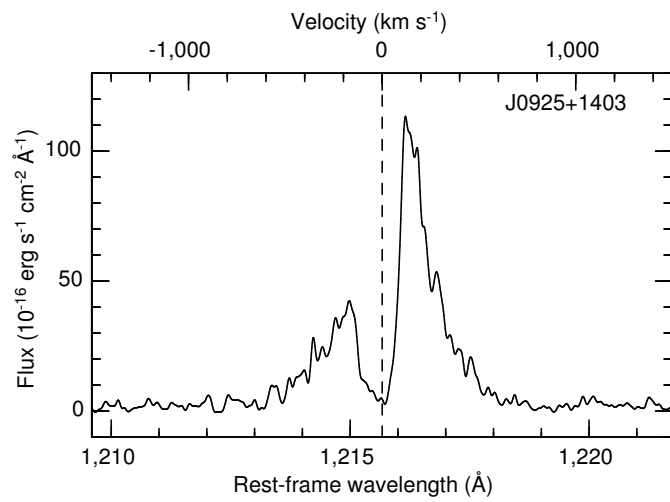


**Figure 3 | The double-peaked  $\text{Ly}\alpha$  emission line in the COS spectrum of J0925+1403.** The center of the line is shown by a vertical dashed line. The small separation of the two emission peaks is indicative of a low HI column density according to radiation transfer models for spherical geometry<sup>21</sup>.



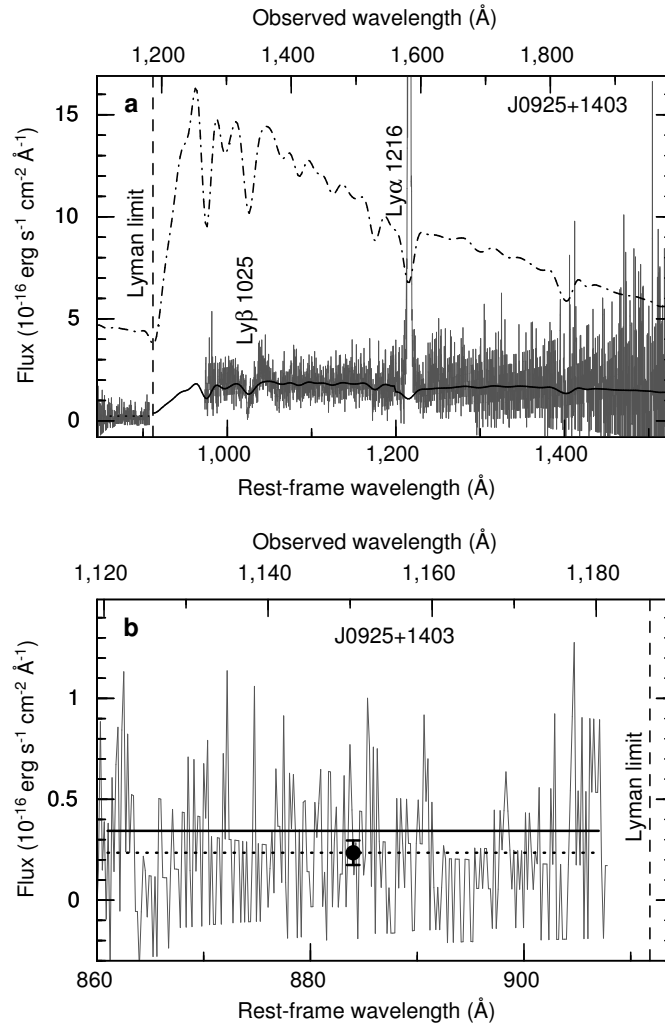


**Figure 4 | The COS spectrum of J0925+1403. a,** On top of the spectrum (grey line) is superposed the modelled spectral energy distribution (SED), reddened by both the Milky Way and internal extinctions (black solid line). The unreddened SED is shown by the dash-dotted line. The dotted line indicates the average observed flux density of the LyC. **b,** The spectrum in the wavelength range 860 – 908 Å. The average observed value with the  $3\sigma$  error bar is shown by filled circle and the dotted line. The solid line represents the LyC level after correction for the Milky Way extinction.

## METHODS

**The sample of compact star-forming galaxies.** A sample of compact star-forming galaxies was selected from the spectroscopic data base of the SDSS Data Release 10 (DR10)<sup>28</sup> by applying the selection criteria: 1)  $R_{50} \leq 3''$ , where  $R_{50}$  is the galaxy’s Petrosian radius, within which 50% of the galaxy’s flux in the SDSS  $r$  band is contained; 2) spiral galaxies were excluded; 3) the emission-line ratio  $[\text{OIII}]\lambda 4959/\text{H}\beta$  is  $\geq 1$  to include only galaxies with high-excitation HII regions, ensuring an accurate determination of their extinctions and chemical compositions; 4) galaxies with AGN activity were excluded using line ratios as described below. Applying these criteria, 5182 galaxies were found in the redshift range  $0 < z < 1$ . Twenty five galaxies of these have  $\text{O}_{32} \geq 5$  and are located in the redshift range 0.30 – 0.35, making direct LyC observations possible. J0925+1403 with equatorial coordinates R.A.=09:25:32.37 and Dec.=+14:03:13.06 was selected for the HST/COS UV observations as one of the brightest objects in the sample of 25 galaxies, with a far-ultraviolet magnitude of 20.7 mag from GALEX. The high rest-frame equivalent width  $\text{EW}_{\text{H}\beta} = 177\text{\AA}$  of the  $\text{H}\beta$  emission line in the SDSS spectrum of J0925+1403 suggests active ongoing star formation.

The  $[\text{OIII}]\lambda 5007/\text{H}\beta - [\text{NII}]\lambda 6584/\text{H}\alpha$  diagnostic diagram<sup>29</sup> of extragalactic objects with emission-line spectra, shown in Extended Data Fig. 1, is useful for discriminating between star-forming galaxies (SFG) and active galactic nuclei (AGN) as ionising sources. The solid line represents the model line<sup>30</sup> that separates the two types of objects. Extended Data Fig. 1 clearly shows that the gas in J0925+1403 is ionised by hot stars in star-forming regions.

**Custom HST/COS G140L Data Reduction.** J0925+1403 was observed with the HST/COS grating G140L for two orbits at a central wavelength of 1280 Å in all four focal-plane offset positions to minimise fixed-pattern noise and to patch grid-wire shadows and other detector blemishes. The data were reduced with CALCOS v2.21 and custom software specifically designed for faint HST/COS targets<sup>31,32</sup>, improving upon previous results on LyC leakage obtained with the default CALCOS pipeline products<sup>11</sup>. As our spectra were taken at COS Detector Lifetime Position 3, we did not employ pulse height filtering to preserve source flux in the presence of detector gain sag from previous usage of COS at the nearby COS Lifetime Position 1. We used boxcar extraction in a narrow 25 pixel rectangular window that preserves spectrophotometry for compact sources (Fig. 2) while minimising the background. The COS background is dominated by detector dark current, which was subtracted in post-processing using scaled dark exposures to account for gain sag in the COS aperture. Specifically, we co-added dark exposures taken in similar orbital conditions within 3 months of the science observations, smoothed the dark current in the COS aperture with a 500-pixel running average to remove Poisson fluctuations, and rescaled the smoothed dark current to the science observations using unilluminated regions of the detector. The resulting estimate of the COS dark current is sufficiently accurate ( $\simeq 5\%$ ) over the wavelength range of interest (1100–1180 Å) to not affect our analysis. Subexposures were co-added by summing raw counts and the smoothed dark current, accounting for differing pixel exposure times due to detector blemishes before converting to flux via the COS calibration curve. This procedure preserves the Poisson counts of faint sources. Airglow contamination

(NI  $\lambda 1134 \text{ \AA}$  and OI  $\lambda 1304 \text{ \AA}$ ) was eliminated by considering only data taken in orbital night in the affected wavelength ranges. We also verified with orbital night data that scattered HI Ly $\alpha$  airglow is negligible in the LyC of J0925+1403. The sum of diffuse open-shutter backgrounds (earthshine, zodiacal light, Galactic emission<sup>33</sup>) is a factor  $\simeq 30$  smaller than the measured flux, leading us to the conclusion that the measured flux is indeed source LyC flux and not unaccounted background.

**Extinction in the optical range.** Using the observed decrement of several hydrogen Balmer emission lines, we corrected the line fluxes relative to the H $\beta$  flux for two effects: (1) reddening adopting the extinction curve<sup>23</sup> and (2) underlying hydrogen stellar absorption. Both are obtained simultaneously by an iterative procedure<sup>34</sup>. The quantity derived from the hydrogen Balmer decrement, is the extinction coefficient  $C_{\text{H}\beta}$ , corresponding to the extinction at the H $\beta$  wavelength  $A_{\text{H}\beta} = 2.512 \times C_{\text{H}\beta}$ . Using the  $A_\lambda/A_V$  fits<sup>23</sup>, we approximate the ratio  $C_{\text{H}\beta}/A_V$  by the relation

$$C_{\text{H}\beta}/A_V = 0.6633 - 0.1317R_V + 0.0294R_V^2 - 0.0024R_V^3 \quad (1)$$

with an accuracy better than 0.1% in the range  $R_V = A_V/E_{B-V} = 2.0 - 4.0$ . We note that  $C_{\text{H}\beta}/A_V$  is weakly dependent on  $R_V$ , decreasing by  $<10\%$  with  $R_V$  increasing from 2 to 4.

The correction for reddening was done in two steps. First, the observed spectrum, uncorrected for redshift, was corrected for the Milky Way extinction with  $A_{V,\text{MW}} = 0.084$  mag and  $R_{V,\text{MW}} = 3.1$  (NASA Extragalactic Database), corresponding to  $C_{\text{H}\beta,\text{MW}} = 0.039$ . Then, the rest-frame spectrum was corrected for the internal extinction of J0925+1403, obtained to be  $C_{\text{H}\beta,\text{int}} = 0.175$  from the hydrogen Balmer decrement, corresponding to  $A_{V,\text{int}} = 0.38$  mag for  $R_{V,\text{int}} = 3.1$  and  $A_{V,\text{int}} = 0.36$  mag for  $R_{V,\text{int}} = 2.4$ . The extinction-corrected emission-line fluxes relative to the H $\beta$  emission line flux and the rest-frame equivalent widths are shown in Extended Data Table 1.

**Element abundances.** The [OIII] $\lambda 4363 \text{ \AA}$  emission line is detected in the SDSS spectrum of J0925+1403. This allows for a reliable oxygen abundance determination using the direct  $T_e$ -method. The temperature  $T_e(\text{OIII})$  is calculated based on the [OIII] $\lambda 4363/(\lambda 4959 + \lambda 5007)$  line ratio<sup>35</sup>. We adopt a two-zone photoionised HII region model: a high-ionisation zone with temperature  $T_e(\text{OIII})$ , where [OIII] lines originate, and a low-ionisation zone with temperature  $T_e(\text{OII})$ , where [OII] lines originate. For  $T_e(\text{OII})$ , we use a model relation between the electron temperatures  $T_e(\text{OIII})$  and  $T_e(\text{OII})$ <sup>35</sup>. Ionic and total abundances of oxygen, nitrogen and neon are derived using expressions for ionic abundances and ionisation correction factors<sup>35</sup>. The derived temperatures and element abundances are shown in Extended Data Table 2. We note that the weak [SII]  $\lambda 6717, 6731$  emission lines, which are used for the electron number density determination, can not be measured because they are located in the noisy part of the J0925+1403 spectrum. Therefore, we adopted the value  $N_e = 100 \text{ cm}^{-3}$ , typical of extragalactic HII regions.

**Fitting of spectral energy distribution and determination of galaxy global parameters.** The luminosity, stellar mass and star-formation rate are important global galaxy characteris-

tics. For the determination of the stellar mass, we follow earlier approach for modelling dwarf galaxies<sup>13,17,27,36</sup>. The method is based on fitting a series of model SEDs to the observed one and finding the best fit. The fit was performed for the SDSS spectrum over the entire observed spectral range of 3900–9200 Å. As the SED is the sum of both stellar and ionised gas emission, its shape depends on the relative contribution of these two components. In J0925+1403, with a rest-frame H $\beta$  equivalent width  $EW_{H\beta} = 177$  Å, the ionised gas continuum is strong and should be subtracted before determining the stellar mass.

We carried out a series of Monte Carlo simulations to reproduce the SED of J0925+1403. To derive the stellar SED, we use a grid of instantaneous burst SEDs in a wide range of ages from 0.0 Myr to 15 Gyr, calculated with *Starburst99*<sup>37,38</sup>. We adopted Geneva stellar evolution tracks for nonrotating and rotating stars<sup>39,40</sup> and Padova stellar evolution tracks<sup>41</sup>. Various models of stellar atmospheres were used<sup>42–45</sup>, and we adopt two different stellar initial mass functions<sup>46,47</sup>. Then the SED with any star-formation history can be obtained by integrating the instantaneous burst SEDs over time with a specified time-varying star-formation rate. The SED of the gaseous continuum was taken into account. It included hydrogen and helium free-bound, free-free, and two-photon emission<sup>48</sup>.

The star-formation history is approximated assuming a recent short burst with age  $t_y < 10$  Myr, which accounts for the young stellar population, and a prior continuous star formation for the older stars during the time interval between  $t_i$  and  $t_f$  ( $t_f < t_i$  and zero age is now). The contribution of each stellar population to the SED was parameterized by the ratio  $b = M_y/M_o$ , where  $M_y$  and  $M_o$  are respectively the masses of the young and old stellar populations. Then the total stellar mass is  $M_* = M_y + M_o$ .

We calculated  $10^5$  Monte Carlo models by randomly varying  $t_y$ ,  $t_i$ ,  $t_f$ , and  $b$ , while other parameters, such as evolutionary tracks, stellar atmosphere models, initial mass function and metallicity are kept fixed. In all cases we used models with metallicities, which best match the metallicity of J0925+1403. We also calculate the equivalent width  $EW_{H\beta}$  for each model. The best solution is required to fulfill two conditions. First, only models, in which the modelled equivalent width  $EW_{H\beta}$  of the H $\beta$  emission line agrees with the observed value within 5 %, were selected. Second, the best modelled SED among selected models for each set of fixed parameters was found from  $\chi^2$  minimization of the deviation between the modelled and the observed continuum in five wavelength ranges, which are free of the emission lines and residuals of the night-sky lines. We found best solutions for 33 combinations of evolutionary tracks, stellar atmosphere models and initial mass functions to investigate the dependence of the LyC flux density on the input parameters. All these solutions provide almost equally good fits at rest-frame wavelengths greater 912 Å and small variations of LyC. The optical spectrum of J0925+1403 with the overlaid SED of one out of the 33 best models is shown in Extended Data Fig. 2. Here we adopted a Salpeter IMF<sup>46</sup>, Padova evolutionary tracks<sup>41</sup> and a combination of stellar atmosphere models<sup>42,43</sup>.

The modelled SED in the UV range is shown in Fig. 4a by a dash-dotted line. We note that the amount of the flux decrease at the Lyman break at a fixed starburst age depends on the adopted

stellar evolution tracks, stellar atmosphere models, and initial mass function. In particular, the Lyman break in models with non-rotating stars is stronger, than in models with rotating stars. However, we find from the SED fitting that the intrinsic flux density  $I(\lambda 912)$  of the LyC varies only by  $\sim 10\%$  in the various sets of models. This is primarily due to the fact that to fit the observed  $\text{EW}_{\text{H}\beta}$ , the starburst age in models with rotating stars should be greater than that in models with non-rotating stars<sup>38</sup>. For young bursts with the age of  $0 - 3$  Myr we obtained the approximate relation  $I(\lambda 912) \sim I(\text{H}\beta)/12$ , which may be used to estimate the intrinsic LyC flux density in galaxies with  $f_{\text{esc}} \ll 1$  without modelling. We also note that this relation is not much changed if continuous star formation is adopted for the young stellar population instead of an instantaneous burst. This is due to the dominant contribution of the  $0 - 3$  Myr stellar population to both the LyC and  $\text{H}\beta$  fluxes, while the contribution of older stars is small.

To derive global characteristics, the observed fluxes were transformed to luminosities adopting the luminosity distance  $1620 \text{ Mpc}^{49}$  and the cosmological parameters  $H_0=67.1 \text{ km s}^{-1}\text{Mpc}^{-1}$ ,  $\Omega_\Lambda=0.682$ ,  $\Omega_m=0.318^{20}$ . Additionally, for the determination of the  $\text{H}\beta$  luminosity  $L_{\text{H}\beta}$  and star formation rate (SFR), the  $\text{H}\beta$  flux density corrected for aperture effects using the relation  $2.512^{r(\text{app})-r}$ , where  $r$  and  $r(\text{app})$  are respectively the SDSS  $r$ -band total magnitude and the magnitude within the round spectroscopic  $3''$  diameter aperture. The aperture correction for J0925+1403 is 1.54. The derived  $\text{H}\beta$  luminosity (Extended Data Table 3) corresponds to a number of ionising photons  $Q_{\text{H}} = 4.94 \times 10^{54} \text{ s}^{-1}$ , in good agreement with the  $Q_{\text{H}}$  obtained from the integration of the number of ionising photons in the modelled intrinsic spectrum (it is only  $\sim 8\%$  lower). The corresponding star-formation rate is derived using the standard Kennicutt relation<sup>50</sup>.

**Reddening law for J0925+1403.** The comparison of the modelled SEDs with the observed photometric and spectroscopic data in the entire UV and optical range allows to verify, which extinction curve is most applicable to J0925+1403. It is known that the extinction curve in the UV range for the Small Magellanic Cloud with oxygen abundance  $12+\log\text{O}/\text{H} \sim 8.1$  is much steeper than the Milky Way extinction curve, and is characterised by  $R_V \sim 2.7^{51-53}$ . On the other hand, the extinction curve in the optical range is insensitive to variations of  $R_V$ . The oxygen abundance of J0925+1403 is lower,  $\sim 7.9$ . Therefore, we may expect the extinction curve in this galaxy to be characterized by an even lower  $R_V$ .

The observed UV and optical spectra are shown in Extended Data Figure 3 by grey lines. Their fluxes are consistent with the SDSS and GALEX photometric fluxes shown by the black symbols. To fit these observational data we reddened the intrinsic modelled SED, keeping the same Milky Way extinction  $C_{\text{H}\beta,\text{MW}} = 0.039$ ,  $R_{V,\text{MW}} = 3.1$ , and the internal extinction  $C_{\text{H}\beta,\text{int}} = 0.175$ , but varying  $R_{V,\text{int}} = 3.1$  (dotted line), 2.7 (dashed line) and 2.4 (solid line). The modelled SEDs were calculated with Padova stellar evolution models<sup>41</sup>, a combination of stellar atmosphere models<sup>42,43</sup> and a Salpeter initial mass function<sup>46</sup>. It is seen that the SEDs reddened with  $R_{V,\text{int}} = 3.1$  and 2.7 do not fit the observed fluxes in the UV range. A higher extinction coefficient  $C_{\text{H}\beta,\text{int}}$  would be needed in the UV. This is difficult to understand in the framework of a model with an uniform dust distribution, characterised by a single value of the extinction.

On the other hand, a SED reddened by the same extinction  $C_{H\beta, \text{int}} = 0.175$ , but with  $R_{V, \text{int}} = 2.4$ , nicely reproduces the observed fluxes. If we use different stellar atmosphere models for the SED modelling, we find somewhat larger  $R_{V, \text{int}}$  in some cases, but not exceeding 2.7.

**Relative Lyman continuum escape fraction.** To compare with other studies, we also estimate the LyC escape fraction from the often-used equation<sup>10</sup>

$$f_{\text{esc}} = f_{\text{esc,rel}} \times 10^{-0.4 \times A_{1500}} = \frac{(f_{1500}/f_{900})_{\text{int}}}{(f_{1500}/f_{900})_{\text{obs}}} \times 10^{-0.4 \times A_{1500}}, \quad (2)$$

where  $f_{900}$  and  $f_{1500}$  are the flux densities at rest-frame wavelengths 900Å and 1500Å, respectively, the subscripts “int” and “obs” denote mean intrinsic and observed flux densities,  $(f_{1500}/f_{900})_{\text{int}} = 1.36$  from our SED fits,  $(f_{1500}/f_{900})_{\text{obs}} = 5.79$ , and  $A_{1500} = 1.58$  mag is the internal extinction at 1500Å (Fig. 4a). From this we obtain the relative escape fraction  $f_{\text{esc,rel}} = 23.6\%$ , and the absolute  $f_{\text{esc}} = 5.5\%$ . The latter value is lower than our above determination for two reasons. First, Eq. 2 does not take into account the fact that the expected extinction at 900Å is higher than at 1500Å. And second, the observed flux density  $f_{900}$  must be corrected for foreground extinction from the Milky Way. Therefore,  $f_{\text{esc}}$  obtained with Eq. 2 is underestimated.

**Code availability.** We have opted not to make the codes for the custom HST/COS data reduction<sup>31</sup> and the galaxy spectral energy distribution fitting<sup>28</sup> available because they are not yet adapted for public use. The *Starburst99* code used to generate spectral energy distribution of single stellar populations is available at <http://www.stsci.edu/science/starburst99/docs/parameters.html>.

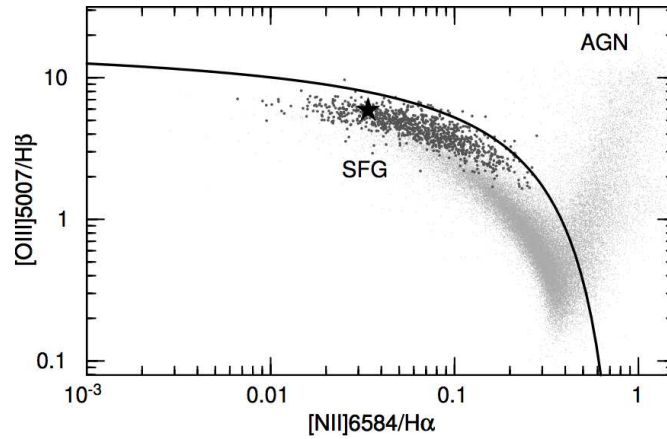
### Additional references

28. Izotov, Y. I., Guseva, N. G., Fricke, K. J. & Henkel, C. On the universality of luminosity-metallicity and mass-metallicity relations for compact star-forming galaxies at redshifts  $0 < z < 3$ . *Mon. Not. R. Astron. Soc.* **451**, 2251–2262 (2015).
29. Baldwin, J. A., Phillips, M. M. & Terlevich, R. Classification parameters for the emission-line spectra of extragalactic objects. *Publ. Astron. Soc. Pacific* **93**, 5–19 (1981).
30. Kauffmann, G. *et al.* Stellar masses and star formation histories for  $10^5$  galaxies from the Sloan Digital Sky Survey. *Mon. Not. R. Astron. Soc.* **341**, 33–53 (2003).
31. Worseck, G. *et al.* The End of Helium Reionization at  $z \simeq 2.7$  Inferred from Cosmic Variance in HST/COS HeII Ly $\alpha$  Absorption Spectra. *Astrophys. J.*, **733**, L24–L29 (2011).
32. Syphers, D. *et al.* HST/COS Observations of Thirteen New HeII Quasars. *Astron. J.*, **143**, 100–111 (2012).
33. Murthy, J. GALEX Diffuse Observations of the Sky: The Data. *Astrophys. J. Suppl.*, **213**, 32–40 (2014).

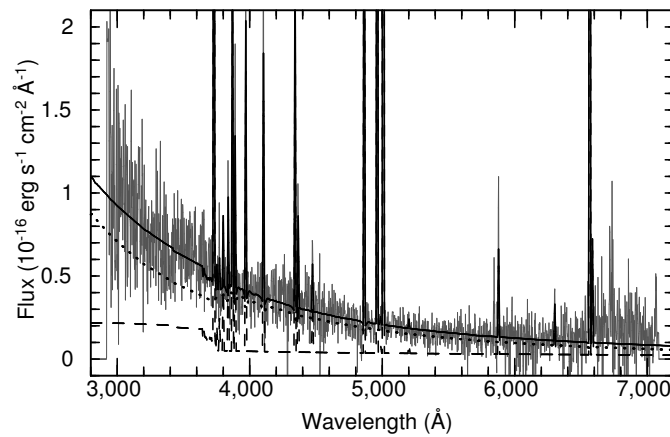
34. Izotov, Y. I., Thuan, T. X. & Lipovetsky, V. A. The primordial helium abundance from a new sample of metal-deficient blue compact galaxies. *Astrophys. J.* **435**, 647–667 (1994).
35. Izotov, Y. I., Stasińska, G., Meynet, G., Guseva, N. G. & Thuan, T. X. The chemical composition of metal-poor emission-line galaxies in the Data Release 3 of the Sloan Digital Sky Survey *Astron. & Astrophys.* **448**, 955–970 (2006).
36. Guseva, N. G., Izotov, Y. I. & Thuan, T. X. Balmer and Paschen Jump Temperature Determinations in Low-Metallicity Emission-Line Galaxies. *Astrophys. J.* **644**, 890-906 (2006).
37. Leitherer, C. *et al.* Starburst99: Synthesis Models for Galaxies with Active Star Formation. *Astrophys. J. Suppl.* **123**, 3–40 (1999).
38. Leitherer, C. *et al.* The Effects of Stellar Rotation. II. A Comprehensive Set of Starburst99 Models. *Astrophys. J. Suppl.* **212**, 14 (2014).
39. Meynet, G., Maeder, A., Schaller, G., Schaerer, D. & Charbonnel, C. Grids of massive stars with high mass loss rates. V. From 12 to 120  $M_{\odot}$  at  $Z=0.001, 0.004, 0.008, 0.020$  and  $0.040$ . *Astron. & Astrophys. Suppl.* **103**, 97–105 (1994).
40. Ekström, S. *et al.* Grids of stellar models with rotation. I. Models from 0.8 to 120  $M_{\odot}$  at solar metallicity ( $Z = 0.014$ ). *Astron. & Astrophys.* **537**, 146 (2012).
41. Girardi, L., Bressan, A., Bertelli, G. & Chiosi, C. Evolutionary tracks and isochrones for low- and intermediate-mass stars: From 0.15 to 7  $M_{\odot}$ , and from  $Z=0.0004$  to 0.03. *Astron. & Astrophys. Suppl.* **141**, 371–383 (2000).
42. Lejeune, T., Buser, R. & Cuisinier, F. Standard stellar library for evolutionary synthesis. I. Calibration of theoretical spectra. *Astron. & Astrophys. Suppl.* **125**, 229–246 (1997).
43. Schmutz, W., Leitherer, C. & Gruenwald, R. Theoretical continuum energy distributions for Wolf-Rayet stars. *Publ. Astron. Soc. Pacific* **104**, 1164–1172 (1992).
44. Hillier, D. J. & Miller, D. L. The Treatment of Non-LTE Line Blanketing in Spherically Expanding Outflows *Astrophys. J.* **496**, 407–427 (1998).
45. Pauldrach, A. W. A. *et al.* Realistic Models for Expanding Atmospheres. ASP Conf. Ser. **131**, 258–277 (1998).
46. Salpeter, E. E. The Luminosity Function and Stellar Evolution. *Astrophys. J.* **121**, 161–167 (1955).
47. Kroupa, P. On the variation of the initial mass function. *Mon. Not. R. Astron. Soc.* **322**, 231–246 (2001).
48. Aller, L. H. *Physics Of Thermal Gaseous Nebulae. Astrophysics and Space Science Library* **112**, Dordrecht, D. Reidel Publishing Co. (1984).

49. Wright, E. L. A Cosmology Calculator for the World Wide Web. *Publ. Astron. Soc. Pacific* **118**, 1711-1715 (2006).
50. Kennicutt, R. C., Jr. Star Formation in Galaxies Along the Hubble Sequence. *Ann. Rev. Astron. Astrophys.* **36**, 189-232 (1998).
51. Bouchet, P., Lequeux, J., Maurice, E., Prévot, L. & Prévot-Burnichon, M. L. The visible and infrared extinction law and the gas-to-dust ratio in the Small Magellanic Cloud. *Astron. & Astrophys.*, **149**, 330-336 (1985).
52. Gordon, K. D. & Clayton, G. C. Starburst-like dust extinction in the Small Magellanic Cloud. *Astrophys. J.*, **500**, 816–824 (1998).
53. Gordon, K. D., Clayton, G. C., Misselt, K. A., Landolt, A. U. & Wolff, M. J. A quantitative comparison of the Small Magellanic Cloud, Large Magellanic Cloud, and Milky Way ultraviolet to near-infrared extinction curves. *Astrophys. J.*, **594**, 279–293 (2003).

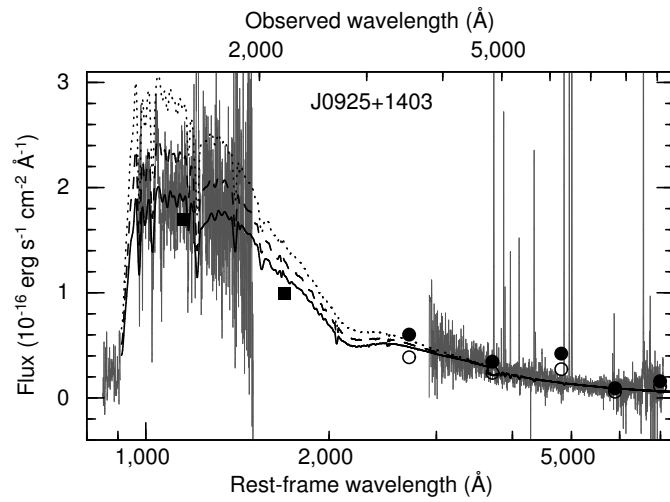




**Extended Data Figure 1 | The diagnostic diagram<sup>29</sup> for narrow emission lines.** The galaxy J0925+1403 is shown by a large filled star, and the Luminous Compact Galaxies<sup>13</sup> by small dark-grey circles. Also, plotted are the 100,000 emission-line galaxies from SDSS DR7 (cloud of light-grey dots). The solid line<sup>30</sup> separates star-forming galaxies (SFG) from active galactic nuclei (AGN).



**Extended Data Figure 2 | SED fitting of the optical spectrum of J0925+1403.** The rest-frame extinction-corrected spectrum is shown by a grey line. The stellar, ionised gas, and total modelled SEDs are shown by black dotted, dashed and solid lines, respectively.



**Extended Data Figure 3 | A comparison of the observed UV and optical spectrum with the modelled SED.** The observed spectrum is shown by a grey line. The total GALEX and SDSS photometric fluxes are represented by filled squares and filled circles, respectively, while the SDSS photometric fluxes within a round spectroscopic aperture of 3'' in diameter are shown by open circles. Modelled SEDs, which are reddened by the Milky Way with  $R_{V,MW} = 3.1$  and internal extinction with different values of  $R_{V,int}$ , are shown by black lines. Dotted, dashed and solid lines correspond to  $R_{V,int} = 3.1, 2.7,$  and  $2.4,$  respectively.

**Extended Data Table 1 | Emission-line fluxes and equivalent widths in the optical spectrum.**

Line	Wavelength (Å)	$100 \times I(\lambda)/I(\text{H}\beta)^\dagger$	EW( $\lambda$ ) (Å)
[OII]	3727	$125.5 \pm 4.6$	77
H9	3835	$9.1 \pm 2.0$	7
[NeIII]	3868	$47.5 \pm 1.9$	33
HeI+H8	3889	$17.1 \pm 2.3$	12
[NeIII]+H7	3968	$32.0 \pm 2.6$	22
H $\delta$	4101	$28.7 \pm 2.3$	22
H $\gamma$	4340	$43.7 \pm 2.5$	36
[OIII]	4363	$11.7 \pm 0.6$	10
HeI	4471	$6.1 \pm 0.5$	6
H $\beta$	4861	$100.0 \pm 3.6$	177
[OIII]	4959	$199.9 \pm 6.7$	306
[OIII]	5007	$608.1 \pm 20.$	1174
HeI	5876	$11.3 \pm 0.7$	22
[OI]	6300	$4.6 \pm 0.5$	11
H $\alpha$	6563	$280.2 \pm 9.9$	732
[NII]	6584	$13.2 \pm 0.8$	26

Footnote:

$^\dagger$ Extinction-corrected flux relative to the extinction-corrected flux  $I(\text{H}\beta) = 4.92 \times 10^{-15} \text{ erg s}^{-1} \text{ cm}^{-2}$  of the H $\beta$  emission line, multiplied by 100.

**Extended Data Table 2 | Physical conditions and chemical composition.**

Parameter	Value
$T_e$ ([OIII]), K	$15010 \pm 410$
$T_e$ ([OII]), K	$14010 \pm 360$
$N_e$ ([SII]), $\text{cm}^{-2}$	$100^\dagger$
$\text{O}^+/\text{H}^+ \times 10^5$	$1.42 \pm 0.11$
$\text{O}^{2+}/\text{H}^+ \times 10^5$	$6.65 \pm 0.50$
$\text{O}/\text{H} \times 10^5$	$8.06 \pm 0.52$
$12 + \log \text{O}/\text{H}$	$7.91 \pm 0.03$
$\text{N}^+/\text{H}^+ \times 10^6$	$1.12 \pm 0.07$
$\text{ICF}(\text{N})^\ddagger$	5.42
$\text{N}/\text{H} \times 10^6$	$6.05 \pm 0.45$
$\log \text{N}/\text{O}$	$-1.12 \pm 0.04$
$\text{Ne}^{2+}/\text{H}^+ \times 10^5$	$1.27 \pm 0.11$
$\text{ICF}(\text{Ne})^\ddagger$	1.08
$\text{Ne}/\text{H} \times 10^5$	$1.37 \pm 0.13$
$\log \text{Ne}/\text{O}$	$-0.77 \pm 0.05$

Footnote:

$^\dagger$  Assumed value.

$^\ddagger$  Ionisation correction factor.

**Extended Data Table 3 | Global characteristics of J0925+1403.**

Parameter	Value
$I_{H\beta}^{\dagger}$	$49.2 \pm 1.3$
Redshift	0.301323
Luminosity distance <sup>‡</sup>	1620
$L_{H\beta}^{\dagger\dagger}$	$(2.32 \pm 0.04) \times 10^{42}$
SFR <sup>‡‡</sup>	52.2
$Q_H^*$	$4.94 \times 10^{54}$
$Q_H(\text{esc})^*$	$3.86 \times 10^{53}$
$t(\text{burst})^{**}$	$2.6 \pm 0.2$
$M_y/M_{\odot}$	$(2.4 \pm 0.3) \times 10^8$
$M_*/M_{\odot}$	$(8.2 \pm 0.7) \times 10^8$

Footnote:

<sup>†</sup>Extinction-corrected flux density in  $10^{-16} \text{ erg s}^{-1} \text{ cm}^{-2}$ .

<sup>‡</sup>in Mpc.

<sup>††</sup>Extinction- and aperture-corrected luminosity in  $\text{erg s}^{-1}$ .

<sup>‡‡</sup>Star-formation rate in  $M_{\odot} \text{ yr}^{-1}$  derived from the  $H\beta$  luminosity<sup>50</sup>.

\* $Q_H$  and  $Q_H(\text{esc})$  are the numbers of LyC photons in  $\text{s}^{-1}$  emitted by massive stars and escaped from the HII region, respectively.

\*\*Burst age in Myr.